Minimum Fuel Coplanar Aeroassisted Orbital Transfer Using Collocation and Nonlinear Programming

By

Yun Yuan Shi* and D. H. Young**
McDonnell Douglas Space System Company
Huntington Beach, California

ABSTRACT

The fuel optimal control problem arising in coplanar orbital transfer employing aeroassisted technology is addressed. The mission involves the transfer from high energy orbit (HEO) to low energy orbit (LEO) without plane change. The basic approach here is to employ a combination of propulsive maneuvers in space and aerodynamic maneuvers in the atmosphere.

The basic sequence of events for the coplanar aeroassisted HEO to LEO orbit transfer consists of three phases. In the first phase, the transfer begins with a deorbit impulse at HEO which injects the vehicle into a elliptic transfer orbit with perigee inside the atmosphere. In the second phase, the vehicle is optimally controlled by lift and drag modulation to satisfy heating constraints and to exit the atmosphere with the desired flight path angle and velocity so that the apogee of the exit orbit is the altitude of the desired LEO. Finally, the second impulse is required to circularize the orbit at LEO. The performance index is maximum final mass.

Simulation results show that the coplanar aerocapture is quite different from the case where orbital plane changes are made inside the atmosphere. In the latter case, the vehicle has to penetrate deeper into the atmosphere to perform the desired orbital plane change. For the coplanar case, the vehicle needs only to penetrate the atmosphere deep enough to reduce the exit velocity so the vehicle can be captured at the desired LEO. The peak heating rates are lower and the entry corridor is wider. From the thermal protection point of view, the coplanar transfer may be desirable. Parametric studies also show the maximum peak heating rates and the entry corridor width are functions of maximum lift coefficient.

The problem is solved using a direct optimization technique which uses piecewise polynomial representation for the states and controls and collocation to represent the differential equations. This converts the optimal control problem into a nonlinear programming problem which is solved numerically by using a modified version of NPSOL. Solutions were obtained for the described problem for cases with and without heating constraints. The method appears to be more robust than other optimization methods. In addition, the method can handle complex dynamical constraints.

---

* Staff Manager, and ** Senior Specialist, Advance Flight System, Advanced Technology.

NOMENCLATURE

A	:	$S\rho_s/2$
C_D	:	drag coefficient
C_{DO}	:	zero-lift drag coefficient
C_L	:	lift coefficient
C_{LR}	:	lift coefficient for maximum lift-to-drag ratio
D	:	drag force
g	:	gravitational acceleration
g_s	:	gravitational acceleration at surface level
H	:	altitude
J	:	performance index
K	:	induced drag factor
L	:	lift force
m	:	vehicle mass
R	:	distance from Earth center to vehicle center of gravity
R_a	:	radius of the atmospheric boundary
R_c	:	radius of the low Earth orbit (LEO)
R_d	:	radius of the high Earth orbit (HEO)
R_E	:	radius of Earth
S	:	aerodynamic reference area
t	:	time
V	:	velocity
T	:	thrust
β	:	inverse atmospheric scale height
γ	:	flight path angle
ψ	:	heading angle
σ	:	bank angle
θ	:	down range angle or longitude
ϕ	:	cross range angle or latitude
μ	:	gravitational constant of Earth
ρ	:	density
Δi	:	orbital plane changes
ΔV	:	characteristic velocity

subscripts

c	:	subscript for circularization or reorbit
d	:	subscript for deorbit
s	:	subscript for surface level

1. INTRODUCTION

In order to have a viable and affordable space program, advanced technology must be exploited and new design concepts must be developed to reduce the size and cost of transportation elements for supporting new mission requirements. One of the new

concepts that has evolved in recent years to advance the cost effectiveness of space transportation systems is the aerodynamically assisted orbit transfer. Such an orbital transfer vehicle is designed with an aerodynamic configuration which can utilize the planetary atmosphere for the purpose of energy management. Numerous studies have demonstrated that the use of the aerobraking can significantly reduce the propulsive velocity requirements for certain class of orbit transfers. Excellent review papers were given by Warberg (Reference 1) and Mease (Reference 10).

In our earlier studies, the fuel optimal control problem arising in a typical nonplanar orbit transfer from HEO to LEO as discussed in most recent publications was addressed. As discussed in References 2 and 15, the aeroassisted orbit transfer vehicle (AOTV) maneuver involves three phases with three propulsive burns or impulses as sketched in Fig.1. The orbital plane change was assumed to perform entirely inside the atmosphere with aeroassistance. Unlike References 2 and 15 , the more general formulation given in Reference 17 does not restrict the orbital plane change to be performed entirely inside the atmosphere. In the first phase , the orbital transfer begins with a deorbit impulse at HEO which injects the vehicle into an elliptic transfer orbit with a plane change at HEO and with the perigee inside the atmosphere. In the second phase, the vehicle is inside the atmosphere and is optimally controlled by the lift and bank angle modulations to perform another orbital plane change and to satisfy the heating rate and other physical constraints. Because of the the energy loss during the atmospheric maneuvers, an impulse is required to initiate the third phase to boost the vehicle back to the final orbital altitude. Finally, the third impulse is applied to circularize the orbit at LEO. Additional plane changes are allowed at the atmospheric exit and the final orbit circulation. In summary, there are three propulsive plane changes associated with three propulsive burns outside the atmosphere and an aeroassisted orbital plane change inside the atmosphere. In Reference 17, simulation results for the general formulation were obtained under the assumption that all trajectories enter the atmosphere at the same ϕ_e, ψ_e, and θ_e. In addition, simulation results were compared with those obtained in Reference 2 and 15, where orbital plane changes are performed entirely inside the atmosphere. These studies provided necessary data base and essential information concerning the effective use of aeroassisted orbital plane changes.

In this paper, the fuel optimal control problem arising in a typical coplanar aeroassisted orbit transfer is addressed. The mission involves the transfer from high energy orbit (HEO) to low enery orbit (LEO) without plane change, The basic approach here is to employ a combination of propulsive maneuvers in space and aerodynamic maneuvers inside the atmosphere. The aeroassisted orbital transfer problem is formulated under the assumption that no orbital plane change is needed. Similar to Reference 15 and 17, the basic sequence of events consists of three phases but only two impulses are needed. In the first phase, the transfer begins with a deorbit impulse at GEO which injects the vehicle into an elliptic transfer orbit with perigee inside the atmosphere. In the second phase, the vehicle is optimally controlled by lift and drag modulation to satisfy heating and other physical constraints and to exit the atmosphere with the desired flight path angle and velocity so that the apogee of the exit orbit is the altitude of the desired LEO. Finally, in the third phase, the second impulse is required to circular the orbit at LEO. The optimal control solutions were all obtained by using the Hermite polynomial and collocation technique

to convert the optimal control problem into a corresponding nonlinear programming (NP) problem which is solved numerically using the optimization code, NZSOL (cf. Reference 12) provided by Gill, which is an improved version of NPSOL (cf. Reference 6), developed at Stanford. This solution method is different from the indirect method such as those discussed in Reference 2,4,7 and 8. Simulation results were then compared with those obtained earlier for different orbital inclination changes in Reference 15 and 17. The details are presented and discussed here. In this paper, simulation results were actually obtained for returns from geosynchronous orbit (GEO) to space station orbit (SSO). It is important that in the future these simulations be extended to include all other realistic flight constraints and to establish baseline optimum trajectory characteristics for GEO to Space station or shuttle, lunar and Mars missions.

2. DIRECT TRAJECTORY OPTIMIZATION WITH COLLOCATION AND HERMITE POLYNOMIALS

In the direct collocation with nonlinear programming approach, the trajectory is approximated by piecewise polynomials, which represent the state and control variables at a number of discrete time points, i.e., nodes. For a given state variable, the state trajectory over a given "segment" between two nodes is taken to be the unique Hermite cubic which goes through the end points of the segments with the appropriate derivatives that are dictated by the differential equations of motion at the endpoints. This is the "Hermite cubic" since it is determined by the states and their derivatives. A collocation is taken at the center of the segment where the derivative given by the Hermite cubic is compared to the derivative obtained from the evaluation of the equations of motion. The difference is termed the "defect" and is a measure of how well the equations of motion are satisfied over the segments. If all the defects are zero, then the differential equations are satisfied at the center collocation points as well as at the endpoints. Figure 2 shows the typical defects between node 1 and node 2.

Let the system of equations of motion be given as

$$X' = f(X,U,D) \tag{2-1a}$$

where X is the state vector, U is the control vector, D is the design parameter vector and (') denotes the differentiation with respect to the time. Let the time over a given segment be T. For the problems mentioned above, one can show that

$$X = (x, y, z, x', y', z', m)$$
$$U = (C_L, \sigma) \tag{2-1b}$$
$$D = (\Delta i_1, \Delta i_2, \Delta i_3)$$

where design parameters are defined here as unknown constants (i.e., three propulsive plane changes) to be determined by the optimizaton processes. Then the Hermite interpolated x-component of the state vector X at the center point is

$$x_c = (1/2)\,(x_1 + x_r) + (T/8)\,[f(X_1,U_1) - f(X_r,U_r)] \tag{2-2}$$

where x_1 and x_r are respectively the x-component of the state vector X at the left and the right nodes. The derivative of the interpolating Hermite cubic at the center point is

$$x_c' = -3/(2T)\,(x_1 - x_r) - (1/4)\,[f(X_1,U_1) + f(X_r,U_r)] \tag{2-3}$$

The defect vector is then calculated as

$$d = f(X_c,U_c) - x_c' \tag{2-4}$$

If x_1, u_1, x_r, and u_r are chosen such that the elements of the defect vector, d, are sufficiently small, the "Hermite polynomials" become an accurate approximation to the

solution of the differential equations of motion (by implicit integration). With the above approach, the differential equations are converted into nonlinear algebraic constraint equations and the optimal control problem can then be solved using the nonlinear programming techques.

3. BASIC EQUATIONS FOR OPTIMAL AEROASSISTED ORBITAL TRANSFER

The aeroassited orbital transfer can be analyzed in three phases , i.e., deorbit, aeroassist (or atmospheric flight), boost and reorbit (or circularization). In each of the phases, a particular set of equations of motion apply.

3.1 Deorbit

Initially, the spacecraft is moving with a circular velocity $V_d = \sqrt{\mu / R_d}$ in a circular orbit of radius R_d, well outside the Earth's atmosphere. Deorbit is accomplished at point D by means of an impulse ΔV_d, to transfer the vehicle from a circular orbit to an elliptic orbit and with perigee low enough for the trajectory to intersect the dense part of the atmosphere. Since the elliptic velocity at D is less than the circular velocity at D, the impulse ΔV_d is executed so as to oppose the circular Velocity V_d. In other words, at point D, the velocity required to put the vehicle into elliptic orbit is less than the velocity required to maintain it in circular orbit. The deorbit impulse ΔV_d causes the vehicle to enter the atmosphere at radius R_a with a velocity V_e and flight path angle γ_e. It is known that the optimal energy loss maneuver from the circular orbit is simply the Hohmann transfer and the impulse is parallel and opposite to the instantaneous velocity vector.

After applying the deorbit impulse and before entering the atmosphere at R_a , the deorbit trajectory is a coasting arc and known integrals of the equations of motion can be used to relate the state vectors at R_a ,the entry into atmosphere to the state vectors right after the deorbit impulse at R_d. Using the principle of conservation of energy and angular momentum at the deorbit point D and the atmospheric entry point E, we get

$$V_e^2 / 2 - \mu / R_a = V_1^2 / 2 - \mu / R_d \tag{3-1}$$

$$R_a V_e \cos(-\gamma_e) = R_d V_1 \tag{3-2}$$

where V_1 is the magnetude of the velovity right after the deorbit impulse ΔV_d and from the above equations we can solve for V_1 and then compute ΔV_d to get

$$V_1 = \sqrt{2\mu(1/R_a - 1/R_d) / \left[(R_d / R_a)^2 / \cos^2 \gamma_e - 1\right]} \tag{3-3a}$$

and

$$\Delta V_d = V_d - V_1 \tag{3-3b}$$

It is easily seen that the minimum deorbit impulse ΔV_{dm} obtained for $\gamma_e = 0$, corresponds to an ideal transfer with the space vehicle grazing the atmospheric boundary. To ensure proper atmospheric entry, the deorbit impulse ΔV_d must be higher than the following minimum deorbit impulse ΔV_{dm}

$$V_{1m} = \sqrt{2\mu(1/R_a - 1/R_d)/\left[(R_d/R_a)^2 - 1\right]} \tag{3-4a}$$

$$\Delta V_{dm} = V_d - V_{1m} \tag{3-4b}$$

Physically, the second term of the above equation corresponds to the apogee velocity of an ellpitic transfer orbit with perigee radius R_a and apogee radius R_d. This elliptic transfer orbit is tangent to the atmosphere boundary at perigee. It will be shown later that the nonlinear constraint equations (3-15) at the atmospheric entry point can also be derived from equations (3-1 and 2).

3.2 Aeroassist

During the atmospheric flight, the vehicle can be optimally controlled by the lift and bank angle modulations to achieve the necessary velocity reduction (due to the atmospheric drag) and the orbital plane change if needed. In the present formulation, only the aeroassisted atmospheric flight need be solved by using the collocation and nonlinear programming techniques discussed earlier in this paper. The solutions in the other phases are provided by the known integral relations of the equations of motion because these arcs are coasting arcs.

Consider a vehicle with the point mass m, moving about a rotating spherical planet. The atmosphere surrounding the planet is assumed to be at rest, and the central gravitational field obeys the usual inverse square law. The equations of motion for the vehicle are given by (Figure 1),

$$\dot{r} = V\sin\gamma \tag{3-5a}$$

$$\dot{\theta} = \frac{V\cos\gamma\cos\psi}{r\cos\phi} \tag{3-5b}$$

$$\dot{\phi} = \frac{V\cos\gamma\sin\psi}{r} \tag{3-5c}$$

$$\dot{v} = \frac{(\eta T\cos\varepsilon - D)}{m} - \frac{\mu\sin\gamma}{r^2} + \omega^2 r\cos\phi\,(\sin\gamma\cos\phi - \cos\gamma\sin\psi\sin\phi) \tag{3-5d}$$

$$\dot{\gamma} = \frac{(\eta T\sin\varepsilon + L)\cos\sigma}{mV} - \frac{\mu\cos\gamma}{Vr^2} + \frac{V\cos\gamma}{r} + 2\omega\cos\psi\cos\phi$$

$$+ \frac{\omega^2 r\cos\phi}{V}(\cos\gamma\cos\phi + \sin\gamma\sin\psi\sin\phi) \tag{3-5e}$$

$$\dot{\psi} = \frac{(\eta T\sin\varepsilon + L)\sin\sigma}{mV\cos\gamma} - \frac{V\cos\gamma\cos\psi\tan\phi}{r} + 2\omega(\tan\gamma\sin\psi\cos\phi - \sin\phi)$$

$$+ \frac{\omega^2 r\cos\psi\sin\phi\cos\phi}{V\cos\gamma} \tag{3-5f}$$

$$\dot{m} = -f(r, V, \eta) \tag{3-5g}$$

where for a given vehicle, the drag D and the lift L are

$$D = \frac{S}{2m}\rho V^2 C_D \tag{3-5h}$$

$$L = \frac{S}{2m} \rho V^2 C_L \tag{3-5i}$$

and the drag and lift coefficients obey the drag-polar relation

$$C_D = C_{DO} + KC_L^2 \tag{3-5j}$$

Also, for an exponential atmosphere, one has

$$\rho = \rho_s \exp(-H\beta) \quad \text{and} \quad H = R - R_E \tag{3-5k}$$

Simulation results obtained here were using the U.S. standard Atmosphere 1976.

For aeroassisted orbital transfer problems considered here, one assumes that, inside the atmosphere, the vehicle is optimally controlled by the aerodynamic forces only. It is assumed that the thrust T is absent and the point mass is constant in this region. Furthermore, no earth rotation was assumed. The later is equivalent to consider the motion with respect to an earth fixed inertial coordinate system (ECI). The plane change or the orbit inclination, *i*, is related to the cross range ϕ and the heading angle ψ as

$$\cos i = \cos\phi \cos\psi \qquad t_e \le t \le t_f \tag{3-6}$$

For coplanar orbital transfer problems considered here, the orbit inclination is assumed to be constant throughout the atmospheric flight.

3.3 Boost and Reorbit

During the atmospheric flight, the vehicle is optimally controlled by the lift and drag modulation to satisfy the heating constraints and to exit the atmosphere with the desired flight path angle and velocity so that the apogee of the exit orbit is the altitude of the desired LEO. Thus, no impulse is required at the exit from the atmosphere to boost the vehicle back to the final orbital altitude at LEO. The vehicle exits the atmosphere at point *F*, with a velocity V_f and the flight path angle γ_f. The additional impulse ΔV_b, required at the exit point *F* for boosting the vehicle into an elliptic transfer orbit with apogee radius R_c is assumed to be zero and the reorbit (or circularization) impulse ΔV_c, required to insert the vehicle into a circular orbit are obtained by using the principle of conservation of energy and angular momentum at the exit point *F* and the reorbit or circularization point *C*. Thus, we have

$$V_f^2/2 - \mu/R_a = V_3^2/2 - \mu/R_c \tag{3-7}$$

$$V_f R_a \cos\gamma_f = R_c V_3 \tag{3-8}$$

where V_f is the velocity at the exit from the atmosphere and V_3 is the velocity at the reorbit point C just before the circularization burn ΔV_c.

Solving for V_f and V_3 from the above equations (3-7) and (3-8) yields

$$V_2 - \sqrt{2\mu(1/R_a - 1/R_c)/\left[1-(R_a/R_c)^2\cos^2\gamma_f\right]} = 0 \tag{3-9}$$

$$V_3 = \sqrt{2\mu(1/R_a - 1/R_c)/\left[(R_c/R_a)^2/\cos^2\gamma_f - 1\right]} \tag{3-10}$$

and ΔV_c can be computed as follows

$$\Delta V_b = 0 \tag{3-11}$$

$$\Delta V_c = V_c - V_3 \tag{3-12}$$

It is interesting to note that V_3 is maximum for $\gamma_f = 0$ and therefore the reorbit impulse ΔV_c ,is minimum for $\gamma_f = 0$. It will be shown later that boundary conditions and nonlinear constraint equations at the exit point F, can be derived in terms of the final orbit characteristics and the final state vectors at the exit as shown in (3-16,17,& 18).

3.4 Performance Index

It is known that the change in speed, ΔV, also called the characteristic velocity, is a convenient parameter to measure the fuel consumption. For minimum-fuel maneuver, the objective is then to minimize the total characteristic velocity. A convenient performance index is the sum of the characteristic velocities for deorbit, boost, and reorbit, as

$$\begin{aligned} J &= \Delta V_d + \Delta V_c \\ &= \Delta V_d(R_d, \Delta i_1, V_e, \gamma_e) + \Delta V_c\,(R_c, \Delta i_3, \gamma_f, V_f) \end{aligned} \tag{3-13}$$

Where, ΔV_d and ΔV_c are the deorbit, and reorbit characteristic velocities respectively, and are given by (3-3, and 12) respectively. Note that for a given final circular orbit, the impulse ΔV_c are completely determined by the state variables V_f and γ_f at the exit of the atmospheric portion of the trajectory. The velocity V_e and the flight path angle γ_e at the atmospheric entry point are dependent only on the magnitude of the deorbit impulse ΔV_d. It follows that the optimal control problem needs to consider only the trajectory segment within the atmosphere subject to the nonlinear constraints and boundary conditions at the atmospheric entry and exit points. In addition, other path constraints such as the peak heating rate have to be satisfied.

3.5 Boundary conditions and constraints

The boundary conditions and constraints for the optimal control problem can be summarized as follows:

- At the entry into atmosphere, the following initial constraints must be satisfied.

$$R = R_a \;;\; \gamma_e \le 0 \tag{3-14a}$$

$$\phi_e = 0, \quad \psi_e = 0, \theta_e = 0, \tag{3-14b}$$

$$\frac{V_e^2}{2}\left[1-\left(\frac{R_a}{R_d}\right)^2 \cos^2(\gamma_e)\right] - \mu\left(\frac{1}{R_a} - \frac{1}{R_d}\right) = 0 \tag{3-15}$$

The first initial constraint is required to ensure the vehicle enters the atmosphere. The second set of boundary conditions assumes that all trajectories enter the atmosphere at the same φ_e, ψ_e and θ_e. In the present formulation, the initial velocity and the flight path angle are unknown and to be determined by the optimization processes subject to the constraint equation (3-15).

- At the exit from atmosphere, the following constraints must be satisfied.

$$R = R_a \;;\; \gamma_f \ge 0 \tag{3-16}$$

$$\frac{V_2^2}{2}\left(1-\frac{R_a^2}{R_c^2}\cos^2\gamma_f\right)-\mu\left(\frac{1}{R_a}-\frac{1}{R_c}\right)=0 \tag{3-17}$$

$$\cos i_f = \cos\phi_f \cos\psi_f = \cos i_e \tag{3-18}$$

Equation (3-16) is required to ensure the vehicle exit the atmophere. The second costraint (3-17) must be imposed to determine the correct V_f and γ_f if ΔV_b, is assumed to be zero as in the coplanar case discussed here. The third constraint (3-18) is required to ensure the orbital transfer is coplanar.

In addition, there are other path constraints ,i.e., constraints must be satisfied along the trajectory such as stagnation point heating rate constraints, altitude constraints, bounds on the control variables abd others

4. STRUCTURE AND SOLUTION OF THE NONLINEAR PROGRAMMING PROBLEM

The direct collocation and Hermite polynomial procedures described above convert optimal control problems into corresponding nonlinear programming problems. Ordinary differential equations are converted into corresponding nonlinear algebraic equations (or nonlinear "defects" constraint equations). These problems can then be solved using nonlinear programming codes.

The variables for the nonlinear programming problem are the collected state vectors and control vectors at the nodes and the time duration of phases. These quantities are assembled into the NLP state vectors

$$X^T = \left[X_1^T, U_1^T, \cdots\cdots X_n^T, U_n^T, t_1, t_2 \cdots\cdots t_k\right] \tag{4-1}$$

where n is the number of nodes and k is the number of phases on the trajectory. The defects and other physical and mathematical constraints are collected into the NLP constraint vector C

$$C^T = \left[d_1^T, d_2^T, \cdots\cdots d_n^T, w_1^T, w_2^T, w_3^T, \cdots\cdots w_j^T\right] \tag{4-2}$$

where d_i is the defect vector and w is a vector of additional problem constraints.

The nonlinear programming code used here is the NZSOL (Reference 12). The NZSOL is an improved version of the NPSOL (Reference 6) , developed by the Stanford Optimization Laboratory and designed to minimize a smooth nonlinear function subject to a set of constraints which may include simple bounds on the variables, linear constraints, and smooth nonlinear constraints The problem is assumed to be stated in the following form:

NP

$$\begin{aligned} &\text{minimize} \quad F(x) \\ &x \in R^n \end{aligned}$$

$$\text{subject to} \quad \ell \le \begin{Bmatrix} x \\ A_L x \\ c(x) \end{Bmatrix} \le u, \tag{4-3}$$

where the objective function $F(z)$ is a nonlinear function, A_L is an m_L, x n constant matrix of general linear constraints, and $c(x)$ is an m_N - vector of nonlinear constraint

functions. the objective function F and the constraint functions are assumed to be smooth, i.e., at least twice-continuously differentiable. (The method of NPSOL will usually solve NP if there are only isolated discontinuities away from the solution).

Note that upper and lower bounds are specified for all the variables and for all the constraints. This form allows full generality in specifying other types of constraints. In particular, the *i-th* constraint may be defined as an equality by setting $\ell_i = u_i$. If certain bounds are not present, the associated elements of ℓ or u can be set to special values that will be treated as $-\infty$ or $+\infty$.

Here we briefly summarize the main features of the method of NZSOL and NPSOL as discussed in Reference 6 because Reference 12 is not available to general public. At a solution of NP, some of the constraints will be active, i.e., satisfied exactly. An active simple bound constraint implies that the corresponding variable is fixed at its bound, and hence the variables are partitioned into fixed and free variables. Let C denote the $m \times n$ matrix of gradients of the active general linear and nonlinear constraints. The number of fixed variables will be denoted by n_{FX}, with n_{FR} ($n_{FR} = n - n_{FX}$) the number of free variables. The subscripts *"FX"* and *"FR"* on a vector or matrix will denote the vector or matrix composed of the components corresponding to fixed or free variables. The details are discussed in Reference 11.

A point x is a first-order Kuhn-Tucker point for NP if the following conditions hold:

(i) x is feasible;

(ii) there exist vectors ζ and λ (the Lagrange multiplier vectors for the bound and general constraints) such that

$$g = C^T \lambda + \zeta, \tag{4-4a}$$

where g is the gradient of F evaluated at x, and $\zeta_j = 0$ if the *j-th* variable is free.

(iii) The Lagrange multiplier corresponding to an inequality constraint active at its lower bound must be non-negative, and non-positive for an inequality constraint active at its upper bound.

Let Z denote a matrix whose columns form a basis for the set of vectors orthogonal to the rows of C_{FR}; i.e., $C_{FR}Z = 0$. An equivalent statement of the condition in terms of Z is

$$Z^T g_{FR} = 0 \tag{4-4b}$$

The vector $Z^T g_{FR}$ is termed the projected gradient of F at x. Certain additional conditions must be satisfied in order for a first-order Kuhn-Tucker point to be a solution of NP.

4.1 The Quadratic Programming Subproblem

Similar to NPSOL, the basic structure of NZSOL involves major and minor iterations. The major iterations generate a sequence of iterates (x_k) that converge to x^*, a first-order Kuhn-Tucker point of NP. At a typical major iteration, the new iterate $\bar{x}$ is defined by

$$\bar{x} = x + \alpha p, \tag{4-5a}$$

where x is the current iterate, the non-negative scalar α is the step length, and p is the search direction. Also associated with each major iteration are estimates of the Lagrange multipliers and a prediction of the active set.

The search direction p is the solution of a quadratic programming subproblem of the form

$$\begin{aligned} &\underset{p}{\text{minimize}} && g^T p + \frac{1}{2} p^T H p \\ &\text{subject to} && \bar{\ell} \le \begin{Bmatrix} p \\ A_L p \\ A_N p \end{Bmatrix} \le \bar{u}, \end{aligned} \tag{4-5b}$$

where g is the gradient of F at x, the matrix H is a positive-definite quasi-Newton approximation to the Hessian of the Lagrangian function and A_N is the Jacobian matrix of c evaluated at x.

The estimated Lagrange multipliers at each major iteration are the Lagrange multipliers from the subproblem (and similarly for the predicted active set) and provide information about the the sensitivity of these NLP problems.

Certain matrices associated with the QP subproblem are relevant in the major iterations. Let the subscripts *"FX"* and *"FR"* refer to the predicted fixed and free variables, and let C denote the m x n matrix of gradients of the general linear and nonlinear constraints in the predicted active set. First, we have available the TQ factorization (Reference 11) of C_{FR} :

$$C_{FR}\, Q_{FR} = (0 \quad T), \tag{4-6}$$

where T is a nonsingular m x m reverse-triangular matrix (i.e., $t_{ij} = 0$ if $i + j < m$), and the non-singular n_{FR} x n_{FR} matrix Q_{FR} is the product of orthogonal transformations. Second, we have the upper-triangular Cholesky factor R of the transformed and re-ordered Hessian matrix

$$R^T R = H_Q \equiv Q^T \bar{H} Q, \tag{4-7}$$

where $\bar{H}$ is the Hessian H with rows and columns permuted so that the free variables are first, and Q is the n x n matrix

$$Q = \begin{pmatrix} Q_{FR} & \\ & I_{FX} \end{pmatrix}, \tag{4-8}$$

with I_{FX} the identity matrix of order n_{FX}. If the columns of Q_{FR} are partitioned so that

$$Q_{FR} = (Z \quad Y), \tag{4-9}$$

the n_Z ($n_Z \equiv n_{FR} - m$) columns of Z form a basis for the null space of C_{FR}. The matrix Z is used to compute the projected gradient $Z^T g_{FR}$ at the current iterate.

As discussed in Reference 6 and 11, a theoretical characteristic of SQP methods is that the predicted active set from the QP subproblem is identical to the correct active set in a neighborhood of x^*. In NPSOL, this feature is exploited by using the QP active set from the previous iteration as a prediction of the active set for the next QP

subproblem, which leads in practice to optimality of the subproblems in only one iteration as the solution is approached. Separate treatment of bound and linear constraints in NPSOL also saves computation in factorizing C_{FR} and H_Q.

4.2 The merit function

Detailed discussions of the merit function are given in Reference 14. In NZSOL and NPSOL, once the search direction p has been computed, the major iteration proceeds by determining a steplength α that produces a "sufficient decrease" in the augmented Lagrangian merit function

$$L(x,\lambda,s) = F(x) - \sum_i \lambda_i(c_i(x) - s_i) + \frac{1}{2}\sum_i \rho_i(c_i(x) - s_i)^2, \tag{4-10}$$

where x, λ and s vary during the line search. The summation terms involve only the nonlinear constraints. The vector λ is an estimate of the Lagrange multipliers for the nonlinear constraints of NP. The non-negative slack variable $\{s_i\}$ allow nonlinear inequality constraints to be treated without introducing discontinuities. The solution of the QP subproblem (4-5) provides a vector triple that serves as a direction of search for the three sets of variables.

4.3 The quasi-Newton updated

Before going into the detailed discussions, it is important to point out that both the NZSOL and NPSOL start by initializing the Hessian matrix H = Identity matrix. Thus at the beginning, the search direction is in the steepest decent direction. No initial curvature information is computed and the curvature information is accumulated through the BFGS quasi-Newton updates. The matrix H in (4-5) is a positive-definite quasi-Newton approximation to the Hessian of the Lagrangian function. At the end of each major iteration, a new Hessian approximation H is defined as a rank-two modification of H. In NPSOL the BFGS quasi-Newton update is used:

$$\bar{H} = H - \frac{1}{s^T H s} H s s^T H + \frac{1}{y^T s} y y^T, \tag{4-11}$$

where $s = \bar{x} - x$ (the change in x).

Rather than modifying H itself, the Cholesky factor of the transformed Hessian H_Q (4-7) is updated, where Q is the matrix from (4-8) associated with the active set of the QP subproblem. The update (4-11) is equivalent to the following update to H_Q :

$$\bar{H}_Q = H_Q - \frac{1}{s_Q^T H_Q s_Q} H_Q s_Q s_Q^T H_Q + \frac{1}{y_Q^T s_Q} y_Q y_Q^T, \tag{4-12}$$

where $y_Q = Q^T y$ and $s_Q = Q^T s$. This update may be expressed as a rank-one update to R and is used to incorporate new curvature information obtained in the move from x *to* $\bar{x}$.

4.4 NZSOL, NPSOL 4.02, and NPSOL 2.1

For those who are interested in applying these NLP codes, there are two publised versions of NPSOL. The NPSOL 4.02 was developed after the NPSOL 2.1 and therefore more reliable and efficient algorithm were incorporated according to Gill (

Reference 12). However, in updating the Cholesky factor, the NPSOL 4.02 updates the whole or complete R while the NPSOL 2.1 updates only the part associated with the Z-space or null space of R. For the problem formulated here ,usually several hundred varibles are involved and the NPSOL 2.1 converges in less computing time. The NZSOL (Reference 12) incorporates not only latest efficient and reliable algorithm but also updates only the part of R associated with the null space of R only. In addition to improve the algorithm of NPSOL, it also adopts the best parts of both NPSOL 2.1 and 4.02.

Finally, it may be interesting to point out that the matrices in the present formulation using collocation and Hermite polynomial are large and fairly sparse. For computational efficiency, it is important to incorporate NLP codes such as MINOS (Reference 13) to take advantage of the special characteristic of the collocation formulation discussed here.

5. NUMERICAL RESULTS AND DATA

The data used in the numerical experiments presented here (c.f. Reference 2 and 9) are summarized as follows:

$$C_{DO} = 0.1 \quad ; \quad K = 1.111 \quad ; \quad m/S = 300 \text{ kg/m}^2 \qquad (5\text{-}1)$$

and the drag polar is

$$C_D = C_{DO} + K * C_L^2 \qquad (5\text{-}2)$$

and other useful data are

$$\rho_a = 1.225 \text{ kg/m}^3; \mu = 3.986\text{x}10^{14} \text{m}^3/\text{sec}^2$$

$$\beta = 1/6900 \text{ m}^{-1}; \; R_E = 6378 \text{ km}$$

$$H_a = 120 \text{ km} \qquad (5\text{-}3)$$

Using the above mentioned data, simulations were carried out

For an AOTV returning from the geosynchronous orbit (GEO) to the space station orbit (SSO) , one has R_d = 42240 km and R_c = 6934 km. Simulation results were obtained for the following parametric studies for different values of C_{LM} .

a) Case 1 (Reference Case). For this reference case , simulation results were obtained under the general formulation that no orbital plane changes are allowed at deorbit, boost,and reorbit impulses and inside the atmosphere. This reference case has the following entry and exit status

Entry status: $H_e = 120$ km; $V_e = 10.315$ km/sec

$\gamma_e = -3.727$ degrees; $\phi_e = 0$; $\psi_e = 0$ (5-4)

Exit status: $H_f = 120$ km; $V_f = 7.952$ km/sec

$\gamma_f = 0.91$ deg; $\phi_f = 0$ deg

$\psi_f = 0$ deg; total flight time = 769.25 sec (5-5)

The characteristic velocities are 1489 meters per seconds and 132 meters per second at the deorbit and the reorbit respectively. The total characteristic velocity is 1621 meters per second. The C_{LMax} is assumed to be 3.0.

b) Case 2 : Simulation results were also obtained for the case where the maximum lift coefficient is assumed to be 4.5. Similar to the reference case, no orbital plane change is allowed. The entry and exit status are summarized as follows:.

Entry status: $H_e = 120$ km; $V_e = 10.3118$ km/sec
$\gamma_e = -3.576$ degrees; $\phi_e = 0$; $\psi_e = 0$ (5-6)

Exit status: $H_f = 120$ km; $V_f = 7.9518$ km/sec
$\gamma_f = 3.576$ deg; $\phi_f = 0$ deg (5-7)
$\psi_f = 0$ deg; $i_f = 0$ degree , total flight time = 673.38 sec

The deorbit characteristic velocity is 1488.91 meters per second and the recirculation characteristic velocity is 131.61 meters per second. The total characteristic velocity is 1620.517 meters per second. It is interesting to observe that all the characteristic velocities are almost the same as those obtained in case 1.

c) Case 3 : Similar to Case 2 , the optimal control solution has a maximum lift coefficient of 2.3 and has the following entry and exit status.

Entry status: $H_e = 120$ km; $V_e = 10.3115$ km/sec
$\gamma_e = -3.814$ degrees; $\phi_e = 0$; $\psi_e = 0$ (5-8)

Exit status: $H_f = 120$ km; $V_f = 7.9515$ km/sec
$\gamma_f = 0.917$ deg; $\phi_f = 0.$deg; $i_f = 0.0$ deg
$\psi_f = 0.0$ deg; total flight time = 857.34 sec (5-9)

d) Case 4. Similar to Case 2, the optimal control solution has a maximum lift coefficient of 0.9 and has the following entry and exit status.

Entry status: $H_e = 120$ km; $V_e = 10.3117$ km/sec
$\gamma_e = -4.154$ degrees; $\phi_e = 0$; $\psi_e = 0$ (5-10)

Exit status: $H_f = 120$ km; $V_f = 7.9509$ km/sec
$\gamma_f = 0.954$ deg; $\phi_f = 0.$deg; $i_f = 0.0$ deg
$\psi_f = 0.0$ deg; total flight time = 1450.67 sec (5-11)

Again, all the characteristic velocities associated with the deorbit, and reorbit impulses for Case 3 and Case 4 are almost the same as Case 1 and Case 2.

Time histories of altitude, velocity, flight path angles,ift coefficient, lift to drag ratio, dynamical pressure, atmospheric density and heating rate for all three cases (Case 1, 2, & 3.) are shown in Figure 3-10. It is important to point out that for the vehicle

considered here, the maximum lift coefficient is 0.9. However, for the simulation results shown here, the maximum lift coeffient is set to be less than 4.5 for paramatric studies.

An interesting observation from the simulation results as shown in Figs. 3 to 10 is that although the total characteric velocity is insensitive to the variation of the maximum lift coefficient , the optimal trajectory is very sensitive. The higher the maximum lift coefficient is the less the vehicle penetrates into the atmosphere and the less the time of flight is needed. The vehicle was flying at the maximum lift coefficient in contrast to previous simulation where the vehicle was flyiny at the maximum lift to drag ratio as shown in Reference 15 and 17. Simulation results shows that for the coplanar orbital transfer the vehicle has only to penetrate the atmosphere deep enough to reduce the exit velocity so that the vehicle will exit the atmosphere at the desired velocity and filght path angle so that the apogee of the exit orbit is the altitude of the desired final LEO.

The heating rate Q_r , along the atmospheric trajectory, is computed for the stagnation point of a sphere of radius of one meter, according to the following relation (Reference 2 and 6)

$$Q_r = K_r \rho^{0.5} V^{3.08} \qquad (5\text{-}12)$$

where the ρ is the atospheric density in kg/km^3, V is the velocity in km/sec and the K_r is the proportionality constant equal to 0.000308. The time history of heating rates for the reference case (Case 1) , Case 2, Case 3, and Case 4 were shown in Fig. 6. These simulation results presented provided enough information that the peak heating rate for coplanar case will be much less than those for cases aeroassisted orbital plane changes are made. As shown in References 15 and 17, one needs less thermal protection materials and more fuel consumption to fly the heat constrained trajectories and therefore by taking into account the weight of thermal protection materials one may find an optimal design to minimize the total vehicle weight.

Another interesting observation from previous simulation results (cf. Reference 15 and 17) is that for given HEO and LEO, the deorbit impulse is almost the same for all the cases simulated here. The total characteristic velocity for a given optimal trajectory is almost completely determined by the boost and the recirculation. In fact, the boost velocity contributes the most to the variation of the total characteristic velocity. Physically, it is obvious as the vehicle makes a larger turn it also loses more energy and therefore needs more velocity to boost it back to the final orbital altitude. Although the total characteristic velocity is insentive to the magnitude of deorbit impulse, the optimal trajectory is very sensitive to ΔV_d. In the coplanar aeroassisted orbit transfer here, the boost impulse is not needed and the deorbit and recirculation impusles are almost the same for all the cases simulated here. Thus the total characteristic velocity is not sensitive to the variation of the maximum lift coefficient. However, the depth of penetration was shown as a function of the maximum lift coefficients.

6. CONCLUDING REMARKS

An excellent survey of the subject was given in Reference 1. Walberg reviewed the problem of optimal aeroassisted orbital transfer with plane change. In a recent paper

by Naidu (c.f. Reference 2), fuel optimal trajectories of aeroassisted orbital transfer with plane change were presented using the so-called multiple shooting method for the case without heating rate constraints and under the assumption that all the plane change was performed entirely in the atmosphere. A brief review of the progress made in this field was also given in Reference 2. In Reference 15 , a similar problem for cases with and without peak stagnation point heating rate constraints was solved using the collocation and nonlinear programming technique. This method is especially suitable for parametrical studies because of its relative insensitivity to initial guesses.

In Reference 17 , simulation results were obtained under a more general formulation that not all the orbital plane changes are made in the atmosphere. It must be noted that the AOTV transfer can be made more efficient propulsively if the plane change is performed partly in the atmosphere and partly in space and the propulsive plane change in space is subdivided into components associated with various impulsive points. All these plane changes were automatically determined by the optimization processes discussed in Reference 17

The above studies provided necessary data bases and essential information concerning how to use and how to combine the propulsive and aeroassited orbital plane changes effectively. In this paper, another group of problems under the assumption no orbital plane change is allowed are investigated. In fact, the present investigation is closely related to the problem of returning from GEO to space station assuming all plane changes are made propulsively outside the atmosphere. As discussed, the charateristics of the flight is quite different from the cases where the orbital plane changes are made inside the atmosphere. In the latter case, the vehicle has to penetrate deeper into the atmosphere to perform the the desired orbital plane change. On the other hand, for the coplanar case, the vehicle needs only to penetrate the atmosphere deep enough to reduce the exit velocity so that the vehicle cn be capture at the desired LEO.

It should be mentioned that the collocation and nonlinear programming technique discussed here was recently applied to another group of orbital transfer problem by Enright and Conway in Reference 3 and the relative insensitivity of this method to the initial guesses was also observed by them. Our basic simulation test bed is the OTIS codes (Reference 5) with an improved and updated nonlinear programming code (NZSOL). All physical models used were documented in Reference 5. Of course, necessary modifications and corrections have to be incorporated to simulate the aerobraking problems discussed here.

It may be worthwhile mentioning that the present problem was actually solved by guessing the initial state and control varibles at four selected points , i.e., the initial point, the final point and two other nodal points along the trajectory inside the atmosphere. The initial state and control variables at other nodes or grid points were simply obtained by linear interpolation. These initial guesses do not have to satisfy either the governing equations or the nonlinear constriants including the defects. Only rough guesses are needed at these four points. Converged solutions were obtained with relative ease. Once a converged solution is obtained, optimal solutions for other cases with differenet inclination changes or different peak heating rate constraints can

be obtained using this converged solution as initial guesses. However, it is important to point out proper scaling of the defects, constraints and variables are essential to get converged solutions. For simulations discussed here, converged solutions were obtained by using as little as 50 nodes. However, in some cases, converged solutions were obtained using 100 nodes. As far as we know, this may be the first time converged soultions were obtained for so many independent variables and nonlinear constraint equations. This also illustrates how powerful the nonlinear programming code and the collocation and Hermite polynomial technique are.

Finally, it is important to mention again that aeroassisted orbital transfer introduces a strong coupling between the vehicle design and the trajectory design as indicated by the simulation data. A trajectory that minimizes fuel mass, without attention to heating , may require the vehicle to have heavy thermal protection systems. As shown here,an optimal design for the total vehicle weight may be obtained as discussed earlier. However, if the aeroassisted transfer is to be prefered to all propulsive transfer, it must offer a reduction in fuel mass greater than the increase in thermal protection mass. As far as minimum fuel is concerned, the reference cases investigated in Reference 17 provided more fuel savings as expected. But for the over all trade-off studies, the peak heating rate, dynamical pressure, maximum g forces, and fuel mass have to be considered. May be, it is also important to point out that the problems investigated here is to assume that all plane changes are propulsive and outside the atmosphere and that the aeroassisted atmospheric flight is planar. This case is most beneficial from the thermal protection point of view and must be considered in the over all trade-off studies.

7. REFERENCES

1. Walberg, G. A., "A Survey of Aeroassisted Orbit Transfer", Journal of Spacecraft and Rockets, Vol. 22, Jan-Feb. 1985, pp 3-18.
2. Naidu, D. S., "Fuel-optimal Trajectories of Aeroassisted Orbital Transfer with Plan Change" AIAA Guidance, Navigation & Control Conference, Boston, MA., August 14-16, 1989.
3. Enright, P. J. and Conway, B. A., "Optimal Finite Thrust Spacecraft Trajectories Using Collocation and Nonlinear Programming", Paper AAS 89-350, AAS/AIAA Astrodynamics Specialist Conference, Stowe, Vermont, August 7-10, 1989.
4. Shi, Y. Y.," Matched Asymptotic Solution For Optimum Lift Controlled Atmospheric Entry ", AIAA JOURNAL, VOL. 9, 1971, PP. 2229-2238.
5. Hardgraves, C. R.and Paris, S. W., " OTIS-Optimal Trajectories by Implicit Integration ", Boeing Aerospace Co., Contract No. F33615-85-C-3009,1988.
6. Gill, P.E., Murray, W., Sanders, M.A., and Wright, M.H., " User's Guide For NPSOL (Version 4.0) : A Fortran Package For Nonlinear Programming ", System Optimization Laboratory, Department of Operation Research, Standford University, Stanford, Claifornia, 1986.
7. Shi, Y. Y., Pottsepp, L., and M. C. Eckstein. " Optimal lift Control of a Hypersonic Lifting Body During Atmospheric Entry ", AIAA Journal, Vol.7, No.12, December,1969..
8. Shi, Y. Y. and Eckstein, M. C., "An Exact Solution for Optimum Controlled Soft Lunar Landing", Astronautica Acta, Vol.16, pp. 9-18, Pergamon Press, New York, 1971.

9. Mease,K.D.and Vinh, N. X.," Minimum-Fuel Aeroassisted Coplanar Orbit Transfer Using Lift-Modulation', AIAA Journal of Guidance and Control, Vol.8,No.1, Jan-Feb. 1985.
10. Mease,K.D., "Optimization of Aeroassisted Orbital Transfer : Current Status", The Journal of the Astronautical Sciences, Special Issue On Hypervelocity Flight,Volume 36, Nos.1/2, January-June,1988.
11. Gill, P.E., and Wright, M.H., " Practical Optimization ", Academic press, London and New York, 1981.
12. Gill, P.E.," NZSOL: An Improved Version of NPSOL", Private Communications , Huntington Beach, California,1989-90.
13. Murtagh, B. A. and Saunders, M.A., " MINORS 5.0 User's Guide", Report SOL 83-20, Department of Operation Research, Standford Research, California, 1983.
14. Gill, P.E., Murray, W., Sanders, M.A., and Wright, M.H.," Some Theoretical Properties of An Augmented Lagragian Merit Function ", Technical Report SOL 86-6R, System Optimization Laboratory, Department of Operation Research, Standford University, Stanford, Claifornia, 1986.
15, Shi, Y. Y. , Nelson, R., L., and Young, D.,H., " Optimal Aeroassisted Orbital Transfer With Plane Change Using Collocation and Nonlinear Programming", Proceedings of 1990 Flight Mechanics / Estimation Theory Symposium, NASA Goddard Space Flight Center, Greenbelt , Maryland , May 22-24, 1990.
16. Jezewski, D. J., " An Efficient Method For Calculating Optimal Free Space, N-Impulse Trajectory", AIAA Journal, Vol. 6, No. 11, November, 1968.
17. Shi, Y. Y. , Young, D..H., & Nelson, R.,L., " Minimum-Fuel Aeroassisted Nonplanar Orbital Transfer Using Collocation and Nonlinear Programming ", Proceedings of the 1990 AIAA/AAS Astrodynamics Specialist Conference, Portland, Oregon, August 22-24, 1990.

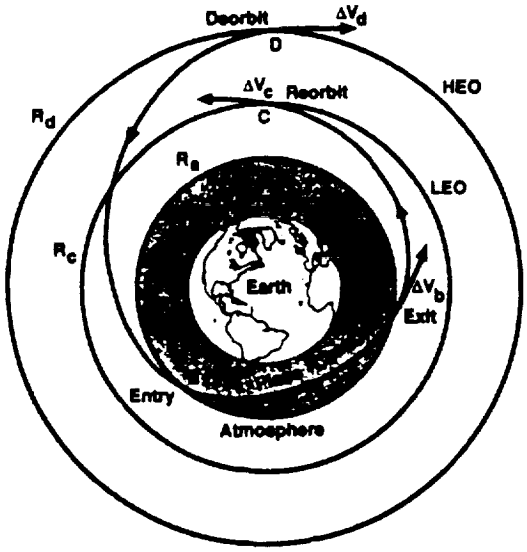

Fig. 1 Aeroassisted Orbital Plane Change

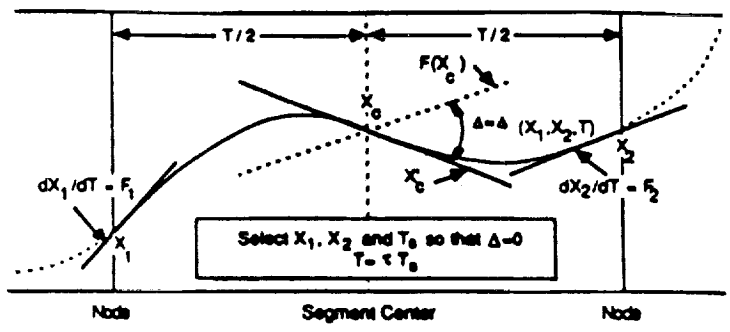

Fig. 2 Collocation and Hermite Approximation

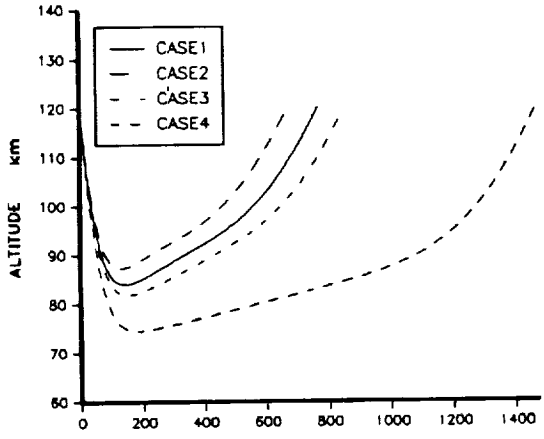

Fig. 3 Time History of Altitude

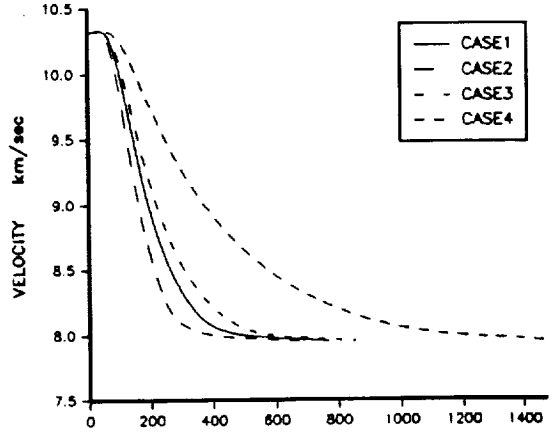

Fig. 4 Time History of Velocity

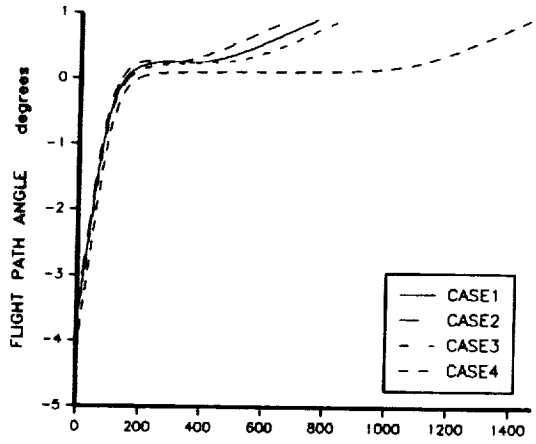

Fig.5 Time History of Flight Path Angle

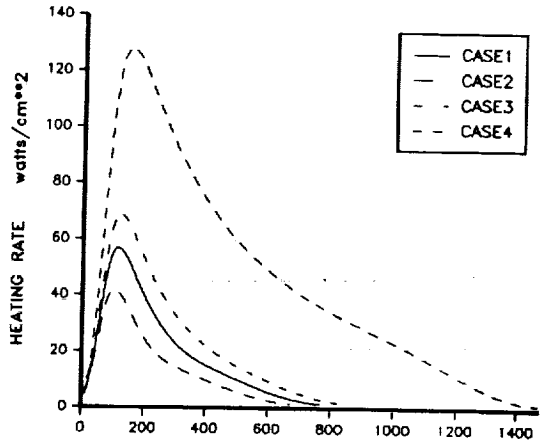

Fig.6 Time History of Heating Rate

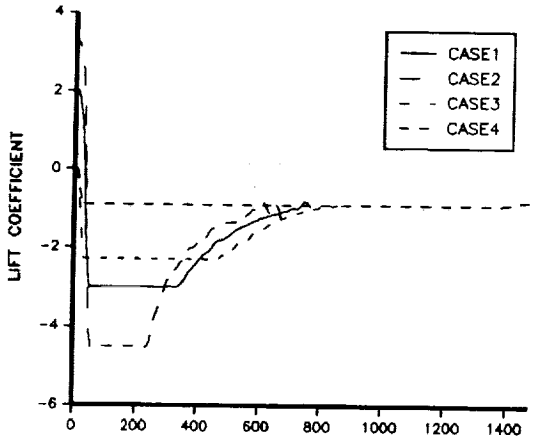

Fig.7 Time History of Lift Coefficient

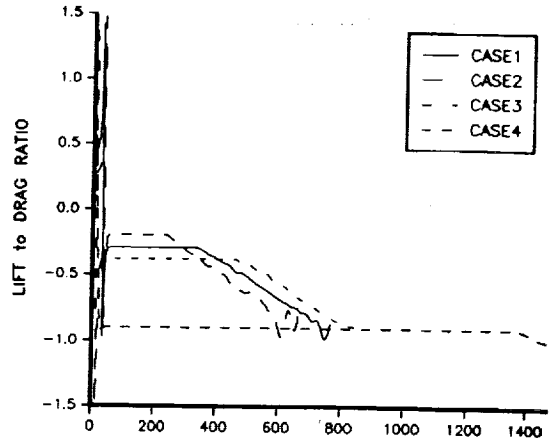

Fig.8 Time History of Lift to Drag Ratio

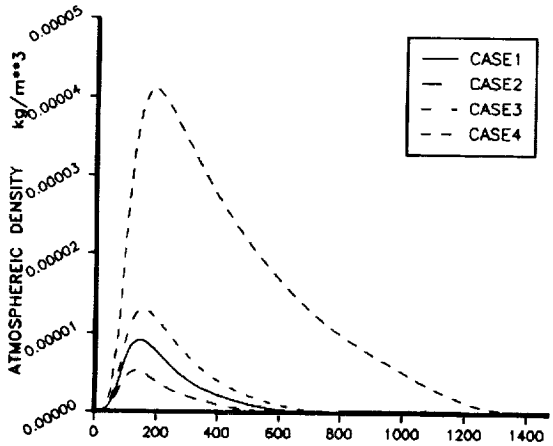

Fig.9 Time History of Atmosphereic Density

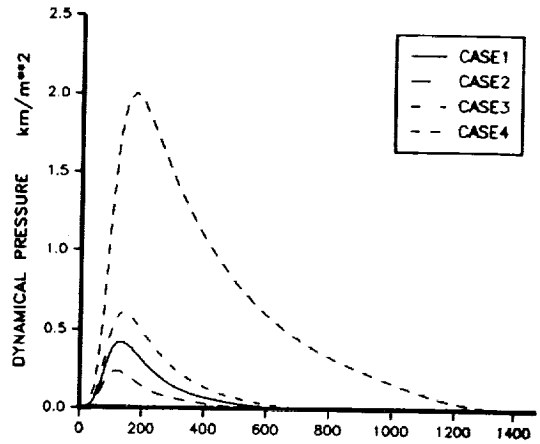

Fig.10 Time History of Dynamical Pressure